Research Square

Preprints are preliminary reports that have not undergone peer review.
They should not be considered conclusive, used to inform clinical practice,
or referenced by the media as validated information.

# Impact of Reservoir Inflow Velocity on Flow Dynamics and Turbine Design in Overtopping Breakwater Energy Conversion Systems

**Yeddid Yonatan Eka Darma**
Institut Teknologi Sepuluh Nopember, Kampus ITS Sukolilo
**Raditya Hendra Pratama**
radi013@brin.go.id

National Research and Innovation Agency (BRIN)
**Ahmad Taufiqur Rohman**
National Research and Innovation Agency (BRIN)
**Samsu Dlukha Nurcholik**
Kalimantan Institute of Technology
**Ippei Oshima**
Tohoku University

**Research Article**

**Keywords:** Non-dimensional analysis, Overtopping breakwater energy conversion, Reservoir inflow velocity, Smoothed particle hydrodynamics, Wave energy conversion

**Posted Date:** June 25th, 2026

**DOI:** https://doi.org/10.21203/rs.3.rs-9637377/v1

**License:** This work is licensed under a Creative Commons Attribution 4.0 International License.
Read Full License

**Additional Declarations:** No competing interests reported.

# Impact of Reservoir Inflow Velocity on Flow Dynamics and Turbine Design in Overtopping Breakwater Energy Conversion Systems

Yeddid Yonatan Eka Darma, Department of Ocean Engineering, Institut Teknologi Sepuluh Nopember, Kampus ITS Sukolilo, Surabaya, East Java, 60111, Indonesia; Department of Ship Manufacturing Engineering, Politeknik Negeri Banyuwangi, Jl. Raya Jember Km. 13, Banyuwangi, East Java, 68461, Indonesia

*Email: yeddidyonatan@poliwangi.ac.id*

Raditya Hendra Pratama, Research Center for Energy Conversion Technology, National Research and Innovation Agency (BRIN), Serpong, Tangerang Selatan, Banten, Indonesia

*Email: radi013@brin.go.id (author for correspondence)*

Ahmad Taufiqur Rohman, Research Center for Energy Conversion Technology, National Research and Innovation Agency (BRIN), Serpong, Tangerang Selatan, Banten, Indonesia

*Email: ahma072@brin.go.id*

Samsu Dlukha Nurcholik, Department of Naval Architecture, Kalimantan Institute of Technology, Balikpapan, East Kalimantan, Indonesia

*Email: dlukha@lecturer.itk.ac.id*

Ippei Oshima, Institute of Fluid Science, Tohoku University, Sendai, Japan; Center for Mathematical Science and Advanced Technology, Japan Agency for Marine-Earth Science and Technology, Yokohama, Japan

*Email: i.oshima@tohoku.ac.jp*

# Impact of Reservoir Inflow Velocity on Flow Dynamics and Turbine Design in Overtopping Breakwater Energy Conversion Systems

**ABSTRACT**

The overtopping breakwater for energy conversion integrates coastal protection with wave energy capture by collecting overtopped water to drive a low-head turbine. While most studies focus on overtopping discharge and reservoir water level, transient flow conditions at the turbine inlet remain insufficiently understood. This study applies a particle-based numerical method to investigate overtopping-induced inflow under regular wave conditions. Two ramp geometries, linear and convex, were analyzed in a numerical wave flume under multiple wave scenarios. The results show that the linear geometry promotes stronger wave run-up and more frequent overtopping, producing higher inflow velocities, whereas the convex geometry enhances energy dissipation and suppresses overtopping. The inflow velocity exhibits systematic dependence on wave characteristics and relative depth conditions, decreasing with increasing wave steepness and increasing with water depth relative to wave height. These findings highlight the importance of velocity-based descriptors for turbine-oriented design in overtopping breakwater systems.

*Keywords*: Non-dimensional analysis; Overtopping breakwater energy conversion; Reservoir inflow velocity; Smoothed particle hydrodynamics; Wave energy conversion

## 1 Introduction

The escalating global demand for sustainable energy solutions has intensified the focus on marine renewable energy, positioning wave energy as a particularly promising option (Astariz & Iglesias, 2015; Lehmann et al., 2017). Among the diverse wave energy conversion technologies, the Overtopping Breakwater for Energy Conversion (OBREC) system offers a distinct and integrated approach by strategically utilizing existing coastal infrastructure for electrical power generation (Contestabile et al., 2020). In this system, overtopping waves are collected into an elevated reservoir, creating a hydraulic head that drives a low-head turbine and converts wave energy primarily into potential energy, with an additional contribution from the overtopping-induced kinetic component of the inflow. Most OBREC performance assessments have therefore focused on reservoir head and overtopping inflow/discharge as the main determinants of power production, whereas the reservoir inlet velocity $V_{res}$ is rarely treated as an explicit hydraulic response variable (Contestabile et al., 2017; Mariani et al., 2021; Musa et al., 2021; Palma et al., 2019; Patrizi et al., 2019; Vicinanza et al., 2014; Van Gent et al., 2022). Although head and discharge are useful for estimating the amount of water captured and the associated hydraulic potential, they do not fully describe the instantaneous flow conditions at the turbine inlet. In OBREC systems, the water entering the reservoir commonly takes the

form of highly transient overtopping jets, splash-up events, and short-duration inflow pulses, so that the resulting inlet forcing may vary substantially even under similar integrated discharge conditions. Consequently, an assessment based only on head or discharge may overlook the dynamic inflow characteristics that are directly relevant to turbine efficiency, loading, and control (Cavallaro et al., 2020; Tedd et al., 2009). This head-centric approach can ignore the inflow speed and its strong short-term fluctuations at the reservoir entrance, which sets the turbine inlet boundary condition, potentially leading to biased interpretation of turbine-relevant forcing (Eskilsson et al., 2015). However, turbine efficiency and control are sensitive to unsteady inflow conditions, which motivates incorporating velocity-based descriptors to better represent the hydraulic forcing delivered to the turbine system (Babarit & Clément, 2006; Falnes, 2002; Falcão, 2010; Kralli et al., 2019).

For instance, Wan et al. (2019) quantified the relationship between sea-state parameters, non-dimensional discharge, and hydraulic efficiency, reinforcing the dominance of discharge-based metrics in OBREC characterization. In contrast, we explicitly treat the reservoir inlet velocity $V_{res}$ as a hydraulic response variable and adopt a gravity-based non-dimensional scaling to represent inlet forcing that is directly relevant to turbine operation beyond discharge alone. Capturing $V_{res}$ requires resolving the highly transient and spatially non-uniform nature of overtopping jets, splash-up, and reservoir entry processes, which are not fully described by integrated discharge metrics.

Accordingly, designing an efficient OBREC system calls for a detailed understanding of overtopping behavior and the associated flow dynamics within the reservoir. In this study, we employ the Smoothed Particle Hydrodynamics (SPH) method to simulate wave propagation towards the OBREC structure and the resulting overtopping processes. The numerical model was verified by comparing the simulated wave characteristics against analytical solutions derived from second-order wave theory, and a suitable particle spacing was selected for the simulations (Iuppa et al., 2016). Additionally, the reservoir crest freeboard $R_r$ and reservoir width $B_r$ were fixed to keep the overtopping conditions consistent across all simulations (Figure 1).

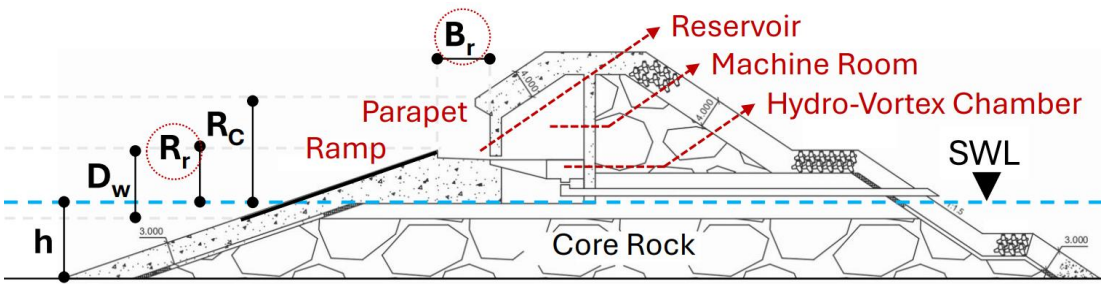



Figure 1 Cross-section of the OBREC system highlighting reservoir crest freeboard ($R_r$) and reservoir width ($B_r$) parameters.

Previous OBREC studies have also shown that ramp geometry plays a fundamental role in controlling wave run-up, overtopping initiation, and the volume of water captured by the reservoir. The ramp shape governs how incident-wave energy is transformed along the slope, affecting flow acceleration, dissipation, and the trajectory of the overtopping jet before entering the reservoir. In general, a linear ramp provides a relatively direct run-up path, whereas a convex ramp modifies the local slope distribution and may alter the balance between wave run-up enhancement and energy loss along the ramp surface (Liu et al., 2017; Martins et al., 2018; Musa et al., 2020). These geometric differences are important because two ramp configurations with similar overtopping discharge may still generate different inflow velocities and different hydraulic conditions at the reservoir entrance. Despite this relevance, the influence of ramp shape on the reservoir inflow velocity remains insufficiently discussed in the OBREC literature.

In recent OBREC studies, geometric features such as ramp profile, crest freeboard ($R_r$), and reservoir layout have been shown to influence wave run-up, the onset of overtopping, and the amount of inflow captured in the reservoir. Building on these findings, this study quantifies the reservoir inflow velocity ($V_{res}$) and its dependence on ramp geometry and incident-wave conditions. Specifically, two ramp configurations, namely linear and convex ramps, are examined to clarify how geometric variation affects overtopping dynamics and the resulting inflow behavior at the reservoir entrance. Using a gravity-based non-dimensional framework, $V_{res}$ is proposed as a key hydraulic response variable to systematically characterize inflow behavior with respect to wave steepness and relative-depth effects, thereby complementing the head- and discharge-based assessment of OBREC performance.

## 2 Methodology

This section details the numerical approach adopted to investigate the overtopping behavior and reservoir flow dynamics of the OBREC system. Our methodology encompasses a two-stage process: an initial model verification to establish simulation accuracy, followed by a comprehensive set of simulations to assess the influence of key design parameters (Iuppa et al., 2016).

This study emphasizes the reservoir inflow velocity ($V_{res}$) as a turbine-relevant hydraulic response variable within a non-dimensional framework. Unlike relative depth and wave steepness, ($V_{res}$) directly characterizes the inlet flow delivered to the reservoir and thus the operating condition seen by the turbine.

The SPH method was employed in this study as a mesh-free method. SPH is a particle-based approach that models fluid flow without using a mesh, representing the fluid domain through individually tracked particles (Monaghan, 2005). While methods such as Volume of Fluid (VOF) generally offer higher accuracy for detailed interface tracking, SPH is

advantageous for problems involving large deformations and free-surface motion. Additionally, SPH is well-suited for parallel computing since it relies mainly on local particle interactions rather than solving global equations (Dalrymple & Rogers, 2009).

### *2.1 Numerical Model and Verification*

In this study, SPH simulations were conducted using the open-source software DualSPHysics, which is suitable for modelling free-surface flows (Monaghan, 2005). The Wendland kernel was selected for its favorable stability and its effectiveness in suppressing non-physical pressure fluctuations and pairing instability, which are important for accurate free-surface flow modelling (Monaghan, 1994).

The fundamental principle of SPH is to approximate the value of a field variable at a given particle location by summing the contributions from all neighboring particles within a smoothing length. The particles interact with one another based on the kernel function ($W$), which determines the weight of each particle's contribution. The distance between particles $i$ and $b$ is defined as $r_i$ - $r_b$, and $h_{sph}$ represents the smoothing length, which defines the interaction radius between particles (Monaghan, 1994). This approximation for a field variable $A$ at particle $i$ is given by:

$$A_i = \sum_b m_b \frac{A_b}{\rho_b} W\left(r_i - r_b, h_{sph}\right) \tag{1}$$

The parameters used in the SPH model are outlined in Table 1, where each parameter is defined with its corresponding description and unit of measurement (Monaghan, 1994).

Table 1 SPH Method Parameters Summary

| Parameter | Description | Unit |
|---|---|---|
| $m_b$ | Mass of particle $b$, calculated from particle volume and fluid density | kg |
| $\rho_b$ | Density of particle $b$, representing the local fluid density at the particle's location | kg m$^{-3}$ |
| $W$ | Smoothing kernel function, which defines the interaction range between particles | - |
| $\|r_i - r_b\|$ | Distance vector between particles $i$ and $b$, used to calculate particle interactions | m |
| $h_{sph}$ | Smoothing length, defining the extent of interaction between particles and determining the resolution of the simulation | m |

Based on the SPH interpolation in Eq. (1), the governing equations are formulated from conservation laws. In particular, the fluid motion is governed by the conservation of momentum. In Eulerian form, the Navier–Stokes momentum equation is expressed as:

$$\frac{\partial v}{\partial t} + (v.\nabla)v = -\frac{1}{\rho}\nabla p + \nu\nabla^2 v + g \tag{2}$$

where $v$ is the velocity vector, $p$ is pressure, $\rho$ is density, $\nu$ is the kinematic viscosity, and $g$ is gravitational acceleration (Monaghan, 1994).

Since SPH is a Lagrangian particle method, Eq. (2) is commonly written using the material derivative $D_v/D_t$. The momentum equation is then discretized in SPH form as:

$$\frac{dv_a}{dt} = \sum_b m_b \left(\frac{p_a+p_b}{\rho_a\rho_b} + \Pi_{ab}\right)\nabla_{ab}W_{ab} + g \tag{3}$$

where the subscripts $a$ and $b$ denote the target and neighboring particles, respectively; $m_b$ is particle mass; $W_{ab}$ is the kernel function; and $\Pi_{ab}$ represents the artificial viscosity term used to stabilize the numerical scheme and capture dissipative effects in free-surface flows (Monaghan, 1994).

To assess the accuracy of the SPH model, simulated wave profiles were compared with analytical solutions from second-order wave theory. The equation represents the final form of the theory, and its full derivation is clearly explained in the literature (Dean & Dalrymple, 1991). The free surface elevation of waves is calculated as:

$$\eta = A_w\, cos(kx - \omega t) + \frac{1}{4}A_w^2 k \frac{cos\, h(kh)(1+2\, cosh^2(kh))}{sinh^3(kh)} cos(2(kx - \omega t)) \tag{4}$$

where, $A_w$ is the wave amplitude (half the wave height), $k$ is the wave number ($2\pi/L$, where $L$ is the wavelength), $\omega$ is the angular frequency, $h$ is the water depth, $t$ is time, and $x$ is the spatial coordinate (Dean & Dalrymple, 1991).

The simulations were conducted using wave conditions scaled from real sea states observed in the southern waters off Bali Island and along the Pacific coast of Japan (Alifdini et al., 2018; Yasuda et al., 2019). Applying a 1:20 physical model scale, a wave height of 0.15 m.

and a wave period of 1.8 s in the simulation represents prototype conditions of 3.0 m wave height and 8.05 s period in the field.

To examine the sensitivity of the SPH model to particle spacing, a series of simulations was conducted using different particle spacings, ranging from 0.01 m to 0.07 m. For each spacing, the simulated wave profiles were compared with the analytical solution based on Eq. (2), and the Root Mean Square (RMS) error was evaluated as shown in Figure 2 (Chai & Draxler, 2014; Gotoh et al., 2004; Trimulyono et al., 2018; Watanabe et al., 2022). Based on the results summarized in Table 2, a particle spacing of 0.03 m, which showed the lowest RMS error, was adopted for all subsequent simulations.

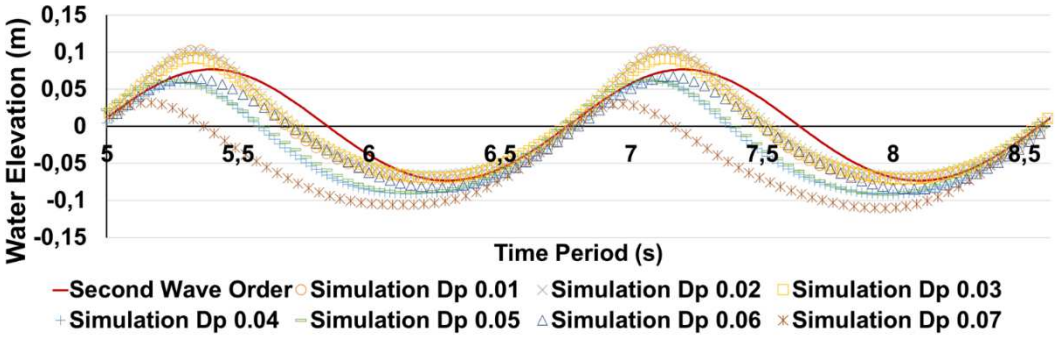



Figure 2 Comparison of simulated wave heights for various Particle Spacing ($D_p$) against analytical results.

Table 2 RMS Errors for SPH Particle Spacing ($D_p$) relative to Second-Order wave theory

| Particle Spacing (m) | RMS Calculation |
|---|---|
| 0.01 | 0.0845 |
| 0.02 | 0.0777 |
| 0.03 | 0.0770 |
| 0.04 | 0.0842 |
| 0.05 | 0.0843 |
| 0.06 | 0.0812 |
| 0.07 | 0.0957 |

Section headings in the main text should be concise and numbered sequentially. Use a decimal number system for subsections.

### *2.2 OBREC System Simulations Set Up*

Numerical simulations were conducted to replicate the performance of the OBREC system in a laboratory-scale wave flume. A side view of this configuration is shown in Figure 3.

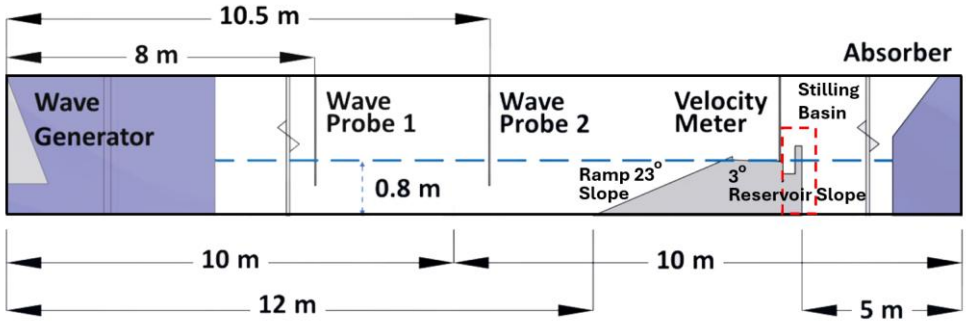



Figure 3 Simulation Setup of OBREC System.

The computational domain represents a wave flume measuring 20 m in length, 2.3 m in width, and 2.5 m in height, with a still water depth ($h$) of 0.8 m. Regular waves were numerically generated at the upstream boundary using the piston-type wavemaker module in DualSPHysics to reproduce different wave conditions. Two configurations of the OBREC structure were modeled, namely a Linear shape and a Convex shape. Both configurations employed a front ramp with a 23° slope, a crest freeboard ($R_r$) of 0.025 m, and a reservoir width ($B_r$) of 0.135 m. Boundary conditions were imposed to replicate the physical constraints of the flume environment (Figure 4).

The simulations were conducted using model-scale wave conditions with significant wave height $H_s$ = 0.15 m and 0.18 m, and peak wave period $T_p$ = 1.59 s, 1.83 s, 2.05 s, and 2.23 s. By combining two OBREC geometries with the four wave periods and two wave heights, a total of 16 simulation cases were analyzed. These simulations enable systematic investigation of overtopping behavior and reservoir flow dynamics under representative wave energy conditions relevant to turbine design.

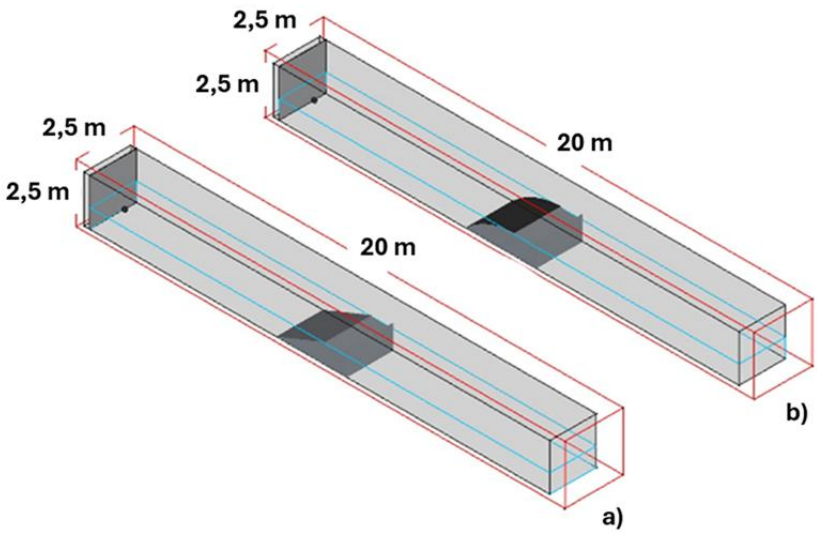



Figure 4 Physical Constraints of the Flume environment: a) Linear Shape and b) Convex Shape of OBREC System

Figure 5 presents the OBREC geometrical details, including the principal dimensions and the effective ramp path length from the ramp toe toward the crest and reservoir entrance. This ramp path length represents the available run-up and acceleration distance of the uprushing water prior to entering the reservoir and provides a physically meaningful basis for interpreting the reservoir inflow velocity ($V_{res}$). For identical incident wave conditions, variations in ramp geometry and flow-path length influence the balance between flow acceleration and energy dissipation along the ramp, leading to differences in $V_{res}$ at the crest and, consequently, differences in overtopping behaviour. Accordingly, the dimensions illustrated in Figure 5 are used to relate the measured $V_{res}$ to the OBREC geometry and to assess the influence of geometric configuration on overtopping under the tested wave conditions.

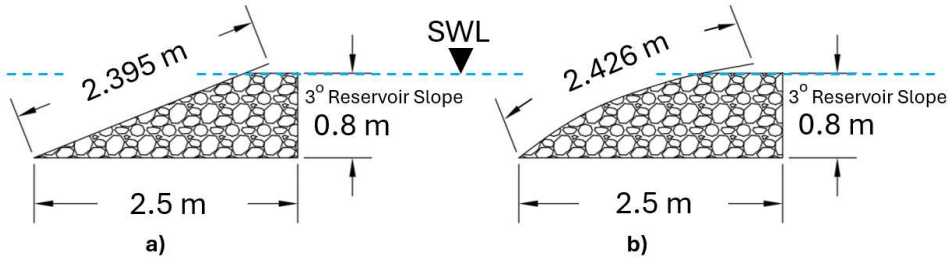



Figure 5 OBREC Geometrical Details: a) Linear and b) Convex Shape of OBREC System without Stilling Basin

### *2.3 Non-Dimensional Analysis*

This study incorporates a non-dimensional analysis based on wave steepness $H/L_m$ and relative-depth scaling $h/H$, $h/L_m$, commonly used to characterize wave-structure interactions and to facilitate comparisons across different scales and environmental conditions (Armono & Hall, 2003). These dimensionless parameters provide a scale-independent measure of overtopping-driven reservoir inflow. It is defined by normalizing the reservoir inflow velocity $V_{res}$ with the gravity-based wave celerity scale $\sqrt{gH}$. For each simulation case, the normalized reservoir inflow velocity was calculated from $V_{res}$, $g$, and $H$ as:

$$\frac{V_{res}}{\sqrt{gH}} \tag{5}$$

where, $g$ is gravitational acceleration, and $H$ is the incident wave height used as the characteristic length scale.

Wave steepness is then introduced to represent wave nonlinearity and energy content:

$$\frac{H}{L_m} \tag{6}$$

Wave steepness $H/L_m$ is a dimensionless descriptor of wave nonlinearity and relative wave shape, and it is therefore relevant for characterizing wave–structure interaction and overtopping-related flow processes. Following Linear wave theory, the mean wavelength $L_m$ was first estimated from the deep-water wavelength and subsequently adjusted for finite water depth (Dean & Dalrymple, 1991) as:

$$L_0 = \frac{gT^2}{2\pi} \tag{7}$$

This estimate was adjusted for intermediate water depths with (Beji et al., 2013):

$$L_m = L_0 \times tanh\left(\frac{2\pi h}{L_0}\right) \tag{8}$$

Finally, the normalized reservoir inflow velocity is examined as a function of dimensionless parameters describing wave steepness and relative-depth effects. In this study, two complementary relative-depth measures are considered: $h/H$, representing the depth-to-wave-height ratio (linked to wave regime and breaking tendency), and $h/L_m$, representing depth relative to wavelength (linked to dispersion and wave transformation). Together with the wave steepness parameter $H/L_m$, these quantities are introduced as complementary dimensionless descriptors that capture different physical aspects of the wave–structure interaction.

Rather than forming a strictly independent Buckingham-π set, these parameters are used to provide physically interpretable descriptors of the hydrodynamic conditions governing reservoir inflow. The combined influence of wave steepness and these relative-depth parameters on the normalized reservoir inflow velocity is expressed in Eq. (9), where $f$ denotes the functional dependence of the normalized inflow velocity on the selected dimensionless parameters. This formulation provides a structured basis for interpreting reservoir inflow behavior across the tested wave conditions.

$$\frac{V_{res}}{\sqrt{gH}} = f\left[\frac{H}{L_m}, \frac{h}{H}, \frac{h}{L_m}\right] \tag{9}$$

where $H/L_m$ is wave steepness, indicating the nonlinearity and energy content, $h/H$ is relative water depth, affecting wave transformation and overtopping behavior, and $h/L_m$ represents the

relative water depth with respect to wavelength, affecting wave interaction and its overtopping behavior.

## 3 Results

### *3.1 Overtopping Behavior and Flow Field Characteristics*

The numerical simulations reproduced overtopping events for both the Linear and Convex OBREC configurations under the tested wave conditions. Figure 6 compares the instantaneous velocity fields for the Linear and Convex ramp geometries at $t$ = 20 s. As shown in Figure 6a, the Linear ramp allows a larger volume of uprushing water to reach and overtop the crest than to the Convex configuration shown in Figure 6b. These differences in flow behavior are further quantified in terms of the reservoir inflow velocity in the following section.

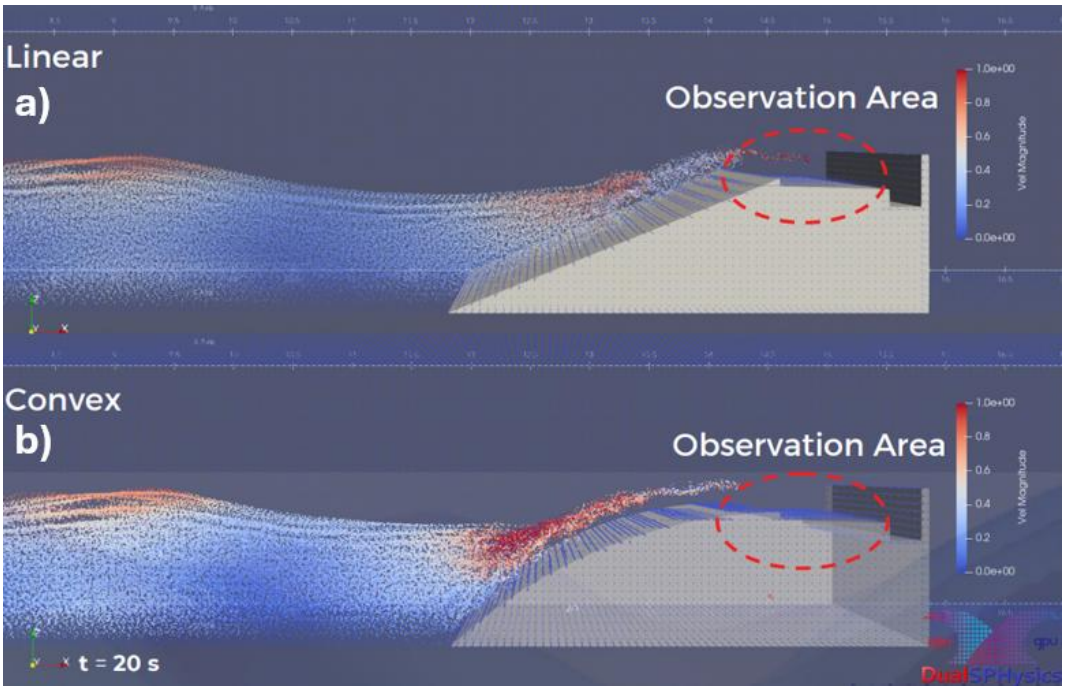



Figure 6 Velocity field comparison for a) Linear and b) Convex OBREC ramp configurations at $t$ = 20 s

### *3.2 Mean Reservoir Inflow Velocity*

Table 3 presents the mean reservoir inflow velocity for simulations conducted with significant wave heights $H_s$ of 0.15 m and 0.18 m across various peak wave periods $T_p$. However, this study observed, several cases with zero velocity, indicating no overtopping under those conditions. For the Linear type, overtopping did not occur under the condition of $H_s$ = 0.15 m and $T_p$ = 1.59 s. Based on this, the minimum condition required to generate overtopping

in the Linear geometry was identified as $H_s$ = 0.15 m with $T_p$ = 1.83 s. Using a 1:20 scale, this corresponds to prototype wave conditions of $H_s$ = 3.0 m and $T_p$ = 8.18 s. As seen in Table 3 and Figure 6, the Convex configuration exhibits zero overtopping in many wave conditions, which can be attributed to this energy loss along the longer ramp.

Table 3 Mean reservoir inflow velocity for linear and convex OBREC ramps under different wave conditions. Values are reported as mean ± standard deviation derived from time-series measurements of overtopping inflow velocity.

| | | **Mean Reservoir Inflow Velocity** | |
|---|---|---|---|
| ***$H_s$* (m)** | ***$T_p$* (s)** | **Linear (m s$^{-1}$)** | **Convex (m s$^{-1}$)** |
| 0.15 | 1.59 | 0 | 0 |
| 0.15 | 1.83 | 0.399 ± 0.062 | 0 |
| 0.15 | 2.05 | 0.468 ± 0.071 | 0 |
| 0.15 | 2.23 | 0.591 ± 0.087 | 0 |
| 0.18 | 1.59 | 0.459 ± 0.068 | 0 |
| 0.18 | 1.83 | 0.467 ± 0.073 | 0 |
| 0.18 | 2.05 | 0.478 ± 0.065 | 0.281 ± 0.052 |
| 0.18 | 2.23 | 0.587 ± 0.081 | 0.512 ± 0.074 |

### *3.3 Non-Dimensional Reservoir Inflow Velocity Results*

Figures 7, 8, and 9 present the relationship between the normalized reservoir inflow velocity, $V_{res}/\sqrt{gH}$, and the dimensionless parameters $H/L_m$, $h/H$, and $h/L_m$, respectively. This result illustrates the role of different non-dimensional parameters in governing momentum transfer from incident waves to the overtopping flow.

Figure 7 shows the relationship between the normalized reservoir inflow velocity $V_{res}/\sqrt{gH}$ and wave steepness $H/L_m$. The results indicate a decreasing trend of $V_{res}/\sqrt{gH}$ with increasing $H/L_m$, as highlighted by the fitted dashed line. Over the tested range ($H/L_m \approx 0.023$ - 0.041), $V_{res}/\sqrt{gH}$ decreases from approximately 0.40 to about 0.32.

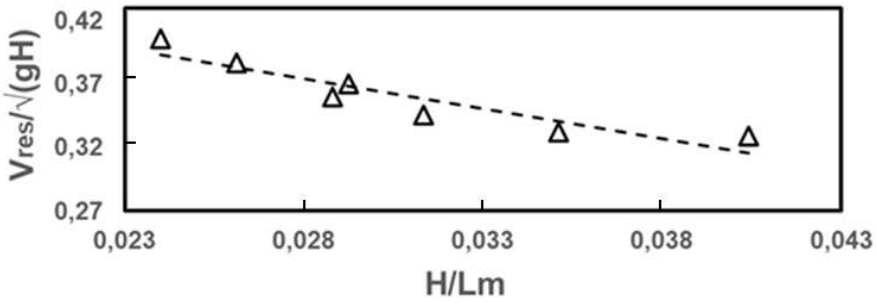



Figure 7 Relationship between normalized reservoir inflow velocity and wave steepness $H/L_m$

In contrast, the $V_{res}/\sqrt{gH}$ versus $h/H$ relationship (Figure 8) shows higher normalized inflow velocities at the larger depth-to-wave-height ratio tested.

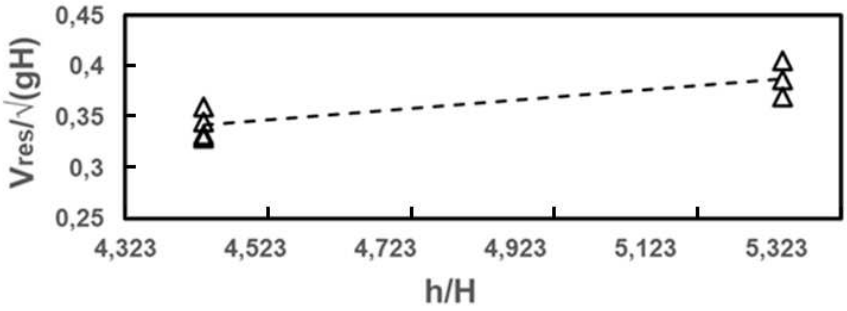



Figure 8 Effect of relative water depth ($h/H$) on normalized reservoir inflow velocity

Finally, the $V_{res}/\sqrt{gH}$ versus $h/L_m$ plot (Figure 9) exhibits a consistent decreasing trend for both $H_s = 0.15$ m and $H_s = 0.18$ m. As $h/L_m$ increases, the normalized inflow velocity decreases, indicating that increasing relative depth with respect to wavelength reduces the effectiveness of momentum concentration at the crest and limits overtopping-driven inflow. Notably, the two wave-height sets follow similar slopes, suggesting that relative-depth effects dominate the observed scaling within the tested range.

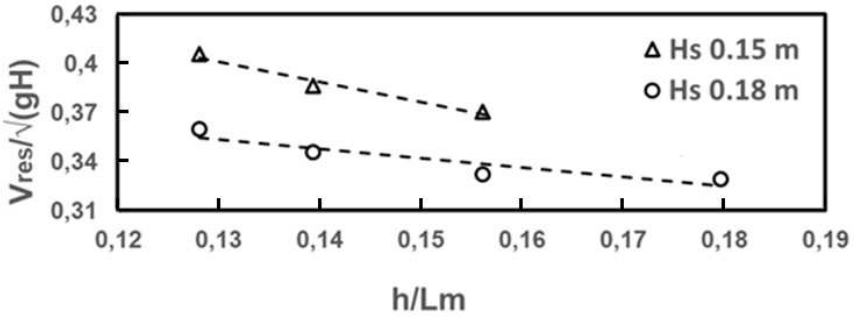



Figure 9 Influence of relative water depth to wavelength ratio ($h/L_m$) on normalized reservoir inflow velocity under different significant wave heights ($H_s$)

## 4 Discussion

### *4.1 Ramp-Geometry Effects on Overtopping Initiation (Linear vs Convex)*

As shown in Figures 6a and 6b, there are differences in the overtopping results. This difference is due to the curvature of the Convex ramp, which tends to deflect or dissipate incoming wave energy, thereby reducing the extent of run-up. In addition to the geometric effect, the Convex ramp induces a 15% longer path length (travel distance) than the Linear

configuration. This extended path length increases the interaction time between the flow and the ramp surface, promoting the development of a thicker boundary layer and larger recirculation zones. Consequently, turbulence intensity and turbulent kinetic energy increase along the Convex ramp, leading to enhanced energy dissipation before the flow reaches the crest. As a result, the ability of the flow to initiate overtopping is reduced under otherwise similar incoming wave conditions. These findings are consistent with the results reported by Musa et al. (2020), who showed that Linear ramp configurations produce higher overtopping discharge than Convex ramps, although their study did not analyze reservoir inflow velocity ($V_{res}$).

### *4.2 Geometry Effects and Reservoir Inflow Velocity Variability*

The current results indicate a potential increase in overtopping velocities with wave period; however, due to the observed variability, this trend cannot be confirmed definitively. To represent this variability explicitly, the associated uncertainty is quantified using the standard deviation, as it directly reflects the physical variability of the unsteady overtopping inflow and is more relevant to turbine design and operational considerations than statistical confidence bounds. In contrast, a more robust trend of increasing overtopping volumes with longer wave periods has been reported by Zhang et al. (2022).

The reduced overtopping in the Convex case (Figure 6b) is consistent with a weaker run-up and diminished high-velocity flow reaching the crest, suggesting enhanced dissipation and/or flow deflection along the curved ramp. The longer travel distance in the Convex shape of the OBREC system leads to increased energy dissipation (Gao et al., 2023). This happens due to frictional losses as the overtopping water travels a longer path along the curved ramp before entering the reservoir. Moreover, this longer flow path can promote stronger near-wall effects, consistent with fluid dynamics principles and evidence from numerical studies on geometrical effects, where frictional drag and turbulent flow increase as the water travels along a more complex surface, thereby enhancing energy dissipation and reducing velocity (Jiao et al., 2024).

In comparison, the Linear ramp provides a shorter run-up path, which reduces frictional and turbulent energy losses and allows a larger fraction of the incoming wave energy to be preserved as flow velocity at the crest. It should be emphasized that the present analysis focuses on reservoir inflow velocity rather than overtopping discharge. Accordingly, comparisons with discharge-centered studies should be interpreted with caution, and the observed trends do not directly contradict the findings of Musa et al. (2020), who reported higher discharge for Convex configurations under higher-energy wave conditions.

At lower wave heights ($H_s$ = 0.15 m and 0.18 m in model scale), overtopping occurs close to the threshold condition, where relatively small additional energy losses can suppress

overtopping entirely. Accordingly, the system response becomes highly sensitive to marginal differences in ramp-induced losses, and no overtopping is observed for the Convex configuration at $H_s$ = 0.15 m, whereas the Linear ramp, with its shorter run-up path, still permits overtopping to occur. This near-threshold sensitivity provides a plausible explanation for the frequent zero-velocity cases reported for the Convex geometry in Table 3. This interpretation is consistent with recent feasibility-level evidence showing that overtopping-based systems may underperform during lower-energy wave periods, emphasizing the sensitivity of overtopping devices to available incident-wave momentum and seasonal wave variability (Sujivakand et al., 2026).

These results indicate that reservoir inflow velocity and overtopping discharge are not necessarily proportional, particularly in low-energy wave regimes. While Convex ramps may enhance discharge under energetic wave conditions by increasing the effective water mass reaching the crest, they may simultaneously suppress overtopping under small-wave conditions due to increased energy dissipation along the longer run-up path. Therefore, velocity-based descriptors offer complementary information to discharge metrics when the objective is turbine-oriented design and operability assessment.

### *4.3 Non-Dimensional Interpretation of Reservoir Inflow Velocity: Effects of Relative Depth and Momentum*

Although Table 3 summarizes the mean reservoir inflow velocity, it does not fully capture the underlying hydrodynamic mechanisms governing reservoir inflow. Therefore, a non-dimensional analysis focusing on the Linear OBREC configuration was conducted to provide deeper insight into the role of relative depth, wave steepness, and depth-to-wave-height ratio on the reservoir inflow velocity. As shown in Figure 7, the normalized inflow velocity $V_{res}/\sqrt{gH}$ decreases with increasing wave steepness $H/L_m$, indicating a systematic dependence of reservoir inflow on incident-wave steepness. This non-dimensional framework allows the observed $V_{res}$ variability to be interpreted consistently across the tested sea states, beyond case-specific dimensional values.

Turning to the relative-depth effect in Figure 8, although only h/H levels are available, the results suggest that when the water depth is sufficiently large relative to the incident wave height, waves can preserve their momentum more effectively while approaching the crest, resulting in a more stable and higher-velocity inflow into the reservoir. Consistent with Figure 8, $V_{res}/\sqrt{gH}$ is higher at the larger $h/H$ level tested, suggesting that relative depth can act as a first-order control on the inlet forcing delivered to the reservoir under the investigated conditions. This interpretation is consistent with previous studies indicating that water depth and relative-depth conditions play a significant role in governing wave transformation and overtopping-related flow behavior. For example, Chen et al. (2022) showed that overtopping

discharge depends strongly on water depth in front of coastal structures, suggesting that relative depth controls wave transformation and overtopping performance when other parameters are kept constant. In addition, factor analysis by other researchers has indicated a positive correlation between water depth and overtopping discharge metrics, further highlighting the role of depth-related parameters in overtopping evaluations. Importantly, these discharge-centered findings provide indirect support for the present velocity-based interpretation, because both discharge and $V_{res}$ reflect the efficiency of momentum transfer into the overtopping flow.

Finally, the $h/L_m$ scaling in Figure 9 shows a consistent decrease in $V_{res}/\sqrt{gH}$ as $h/L_m$ increases for both tested $H_s$ levels, and the similar slopes indicate that relative-depth effects expressed through $h/L_m$ dominate the scaling within the investigated range. Overall, the systematic trends observed across Figures 7-9 align with prior research emphasizing the controlling role of wave momentum and dimensionless parameters on overtopping processes. In particular, Setayesh and Moghim (2025) employed a momentum flux-based analytical-experimental approach for OBREC, highlighting the significant influence of wave momentum in overtopping behavior and supporting the importance of relative depth effects in scaling overtopping inflow velocity. Taken together, the combined trends in Figures 7-9 reinforce the need to treat velocity-based descriptors as complementary to discharge metrics when the objective is turbine-oriented assessment of reservoir inlet conditions and power take-off (PTO) operability.

### *4.4 Implications for Turbine-Integrated OBREC Design*

In most overtopping and OBREC-related studies, reservoir inflow is predominantly characterized using discharge-based metrics, because the primary objective is typically the assessment of overtopping performance and energy potential rather than the hydraulic design of the energy conversion system (Adibhusana et al., 2023; Han et al., 2018; Liu et al., 2017; Nguyen et al., 2020). However, once OBREC is coupled to a turbine, discharge alone is insufficient to describe the forcing conditions at the turbine inlet. Turbine operation and efficiency depend on the hydraulic head and the flow dynamics, meaning that the incoming flow velocity and its associated momentum become critical design variables, not simply secondary outcomes.

This turbine-oriented perspective is consistent with field-oriented OBREC turbine studies. Contestabile et al. (2023) explicitly treated the PTO performance as a function of reservoir water level (head) and the hydraulic conditions driving the turbine, noting that the turbine is activated only when the reservoir free surface exceeds a threshold, and that the operational regime is governed by the coupled variability of head and inflow conditions within the PTO hydraulic system. In other words, the turbine-integrated OBREC is essentially a head–flow–control problem rather than a discharge-only overtopping problem, implying that the inflow

velocity is directly relevant to efficiency, activation/deactivation behavior, and robust PTO selection.

In this context, the present results indicate that the non-dimensional reservoir inflow velocity, $V_{res}/\sqrt{gH}$, exhibits systematic trends with key non-dimensional wave parameters, indicating that velocity variations are not negligible and should be explicitly considered in turbine-oriented analyses. This argument also complements momentum-based overtopping formulations such as Setayesh and Moghim (2025), who relate non-dimensional discharge to wave momentum flux. While such formulations improve physical consistency by acknowledging momentum transfer, they still remain discharge-centered and do not explicitly resolve the reservoir inflow velocity field that governs turbine inlet conditions. Therefore, incorporating $V_{res}$ as an explicit design parameter provides a more direct bridge between wave-driven overtopping hydraulics and PTO design, particularly when turbine activation thresholds and efficiency envelopes are sensitive to hydraulic conditions (Contestabile et al., 2023).

Moreover, the role of geometry becomes crucial when velocity is treated as a design variable. Referring to Figure 6 and the measured $V_{res}$ data (Table 3), the Linear geometry yields a typical velocity band of approximately 0.4-0.6 m $s^{-1}$, and within the tested sea states, this band is associated with a broader occurrence of overtopping inflow conditions than the Convex geometry. Interpreted from a turbine-operability standpoint, this suggests that the Linear geometry provides a wider operational range, reducing the risk that the turbine becomes inactive under low-energy wave conditions; conversely, the Convex geometry tends to concentrate operation into higher-energy states, making turbine deactivation more likely when incident wave energy is low. This pattern is aligned with broader coastal hydraulics evidence that changes in geometrical characteristics (shape features, characteristic lengths along the flow path) can significantly modify run-up and wave energy dissipation pathways. Jiao et al. (2024), for example, showed that modifying block geometrical characteristics affects wave run-up reduction and dissipation performance, reinforcing the general principle that geometric changes can meaningfully reshape the near-surface flow and energy transformations relevant to overtopping processes.

Taken together, these findings support the central implication of this study: the normalized reservoir inflow velocity, $V_{res}/\sqrt{gH}$, should be treated as a governing hydraulic parameter for turbine-integrated OBREC systems, not merely a derived by-product of overtopping. Explicit inclusion of $V_{res}$ enables more physically consistent turbine selection and performance optimization, particularly for defining activation thresholds, expected operational envelopes, and reliability under variable sea states, thereby bridging the gap between overtopping hydrodynamics and PTO design (Darma et al., 2026; Zakaria & Mukhtasor, 2025).

## 5 Conclusion

SPH simulations show that overtopping-driven reservoir inflow in the Linear OBREC configuration depends systematically on wave transformation and relative-depth effects. The non-dimensional results indicate that the normalized inflow velocity, $V_{res}/\sqrt{gH}$, decreases with increasing wave steepness $H/L_m$ and with increasing relative depth-to-wavelength ratio $h/L_m$, while increasing with the depth-to-wave-height ratio $h/H$. This combined pattern suggests that, within the tested range, steeper waves and larger $h/L_m$ promote earlier breaking and enhanced dissipation along the ramp, reducing the effective momentum transferred into the reservoir, whereas larger $h/H$ supports momentum preservation toward the crest and yields higher inflow velocities. Importantly, the similarity of trends across $H_s$ levels implies that relative-depth scaling governs $V_{res}$ more strongly than wave height alone under the investigated conditions. Accordingly, $V_{res}$ should be treated as an explicit hydraulic response variable in OBREC hydrodynamic assessments, as it provides a turbine-relevant inflow descriptor that cannot be inferred from discharge alone and enables more physically consistent performance evaluation and design optimization.

Although the present SPH results clarify the systematic dependence of $V_{res}/\sqrt{gH}$ on wave transformation and relative-depth scaling, further work is required to generalize these findings across a wider design space. Future research should investigate additional OBREC flow-path geometries (e.g., variations in ramp profile, crest shape, and reservoir entry configuration) to quantify how geometric modifications alter momentum delivery into the reservoir, and extend the numerical campaign to multiple still-water depth levels to directly assess the sensitivity of $V_{res}$ to depth-dependent transformation regimes. These extensions would strengthen turbine-oriented design guidance by mapping inflow-velocity operability across geometry–depth combinations and improving the robustness of performance optimization.


## Acknowledgements

The authors acknowledge the institutional support provided by Institut Teknologi Sepuluh Nopember, Politeknik Negeri Banyuwangi, the National Research and Innovation Agency (BRIN), Kalimantan Institute of Technology, and Tohoku University, which facilitated the completion of this research.

## Funding

This work was supported by the IFS Collaborative Research Project 2025 under grant number J25R002. The funding supported the numerical modelling, data analysis, and collaborative research activities conducted in this study.

**Notation**

| | |
|---|---|
| $a$ | Index of target particle (-) |
| $A_b$ | Area associated with particle b ($m^2$) |
| $A_w$ | Wave amplitude (m) |
| $b$ | Index of neighboring particle (-) |
| $B_r$ | Reservoir width (m) |
| $D_p$ | Particle spacing (m) |
| $D_w$ | Local water depth at the structure (m) |
| $g$ | Gravitational acceleration ($m\ s^{-2}$) |
| $h$ | Still water depth (m) |
| $h_{sph}$ | SPH smoothing length (m) |
| $H$ | Incident wave height (m) |
| $H_s$ | Significant wave height (m) |
| $H/L_m$ | Wave steepness (-) |
| $h/H$ | Depth-to-wave-height ratio (-) |
| $h/L_m$ | Relative depth-to-wavelength ratio (-) |
| $k$ | Wave number ($m^{-1}$) |
| $L$ | Wavelength (m) |
| $L_0$ | Deep-water wavelength (m) |
| $L_m$ | Mean wavelength (m) |
| $m_b$ | Mass of neighboring particle b (kg) |
| $p$ | Pressure (Pa) |
| $P_b$ | Pressure at particle b (Pa) |
| $r_b$ | Position vector of particle b (m) |
| $r_i$ | Position vector of particle i (m) |
| $R_c$ | Crest elevation (m) |
| $R_r$ | Crest freeboard (m) |
| $t$ | Time (s) |
| $T$ | Wave period (s) |
| $T_p$ | Peak wave period (s) |
| $v$ | Velocity vector ($m\ s^{-1}$) |
| $V_{res}$ | Reservoir inflow velocity ($m\ s^{-1}$) |
| $V_{res}/\sqrt{gH}$ | Normalized reservoir inflow velocity (-) |
| $W$ | Kernel function (-) |
| $W_{ab}$ | Kernel interaction (particles a and b) (-) |
| $x$ | Spatial coordinate (m) |

| | |
|---|---|
| $\nu$ | Kinematic viscosity ($m^2\ s^{-1}$) |
| $\omega$ | Angular frequency (rad $s^{-1}$) |
| $\Pi_{ab}$ | Artificial viscosity term (-) |
| $\rho$ | Fluid density (kg $m^{-3}$) |
| $\rho_b$ | Density of particle b (kg $m^{-3}$) |
| $\eta$ | Free surface elevation relative to still water level (m) |

**References**


Adibhusana, M. N., Lee, J. I., Kim, Y. T., & Ryu, Y. (2023). Study of overtopping flow velocity and overtopping layer thickness on composite breakwater under regular wave. *Journal of Marine Science and Engineering*, 11(4), 823. https://doi.org/10.3390/jmse11040823

Alifdini, I., Iskandar, N. A. P., Nugraha, A. W., Sugianto, D. N., Wirasatriya, A., & Widodo, A. B. (2018). Analysis of ocean waves in three sites potential areas for renewable energy development in Indonesia. *Ocean Engineering*, 165, 34–42. https://doi.org/10.1016/j.oceaneng.2018.07.013

Armono, H. D., & Hall, K. R. (2003). Wave transmission on submerged breakwaters made of hollow hemispherical shape artificial reefs. In *Proceedings of the Canadian Coastal Conference* (pp. 313–322).

Astariz, S., & Iglesias, G. (2015). The economics of wave energy: A review. *Renewable and Sustainable Energy Reviews*, 45, 397–408. https://doi.org/10.1016/j.rser.2015.01.061

Babarit, A., & Clément, A. H. (2006). Optimal latching control of a wave energy device in regular and irregular waves. *Applied Ocean Research*, 28(2), 77–91. https://doi.org/10.1016/j.apor.2006.05.002

Beji, S. (2013). Improved explicit approximation of linear dispersion relationship for gravity waves. *Coastal Engineering*, 73, 11–12. https://doi.org/10.1016/j.coastaleng.2012.10.002

Cavallaro, L., Iuppa, C., Castiglione, F., Musumeci, R. E., & Foti, E. (2020). A simple model to assess the performance of an overtopping wave energy converter embedded in a port breakwater. *Journal of Marine Science and Engineering*, 8(11), 858. https://doi.org/10.3390/jmse8110858

Chai, T., & Draxler, R. R. (2014). Root mean square error (RMSE) or mean absolute error (MAE)? Arguments against avoiding RMSE in the literature. *Geoscientific Model Development*, 7(3), 1247–1250. https://doi.org/10.5194/gmd-7-1247-2014, 2014.

Chen, S., Chen, H., Peng, C., Wang, Y., & Hu, Y. (2022). Analysis of factors influencing wave overtopping discharge from breakwater based on an MIV-BP estimation model. *Water*, 14(19), 2967. https://doi.org/10.3390/w14192967

Contestabile, P., Crispino, G., Di Lauro, E., Ferrante, V., Gisonni, C., & Vicinanza, D. (2020). Overtopping breakwater for wave energy conversion: Review of state of the art, recent advancements and what lies ahead. *Renewable Energy*, 147, 705–718. https://doi.org/10.1016/j.renene.2019.08.115

Contestabile, P., Iuppa, C., Di Lauro, E., Cavallaro, L., Andersen, T. L., & Vicinanza, D. (2017). Wave loadings acting on innovative rubble mound breakwater for overtopping wave energy conversion. *Coastal Engineering*, 122, 60–74. https://doi.org/10.1016/j.coastaleng.2017.02.001

Contestabile, P., Rubino, L., Crispino, G., Mariani, A., Unich, A., Gisonni, C., & Vicinanza, D. (2023). A new seawater low-head turbine for the OBREC. In *Proceedings of the European Wave and Tidal Energy Conference* (Vol. 15). https://doi.org/10.36688/ewtec-2023-548

Dalrymple, R. A., & Rogers, B. D. (2009). Numerical modeling of water waves with the SPH method. Coastal Engineering, 56(1), 69–80. https://doi.org/10.1016/j.coastaleng.2005.10.004

Darma, Y. Y. E., Rahmawati, S., Rosyid, D. M., Pratama, R. H., & Kusuma, A. I. (2026). Overview of advancements in overtopping breakwater for wave energy conversion (OBREC): Harnessing coastal power for renewable energy and enhanced coastal protection. *Renewable and Sustainable Energy Reviews*, 226, 116399. https://doi.org/10.1016/j.rser.2025.116399

Dean, R. G., & Dalrymple, R. A. (1991). Water wave mechanics for engineers and scientists. World Scientific.

Eskilsson, C., Palm, J., Kofoed, J. P., & Friis-Madsen, E. (2015). CFD study of the overtopping discharge of the Wave Dragon wave energy converter. In *Renewable Energies Offshore* (pp. 287–294).

Falcão, A. F. O. (2010). Wave energy utilization: A review of the technologies. *Renewable and Sustainable Energy Reviews*, 14(3), 899–918. https://doi.org/10.1016/j.rser.2009.11.003

Falnes, J., & Kurniawan, A. (2020). *Ocean waves and oscillating systems: Linear interactions including wave-energy extraction*. Cambridge University Press.

Gao, Y., Ren, L., & Wang, L. (2023). Experimental investigation of wave propagation and overtopping over seawalls on a reef flat. *Journal of Marine Science and Engineering*, 11(4), 836. https://doi.org/10.3390/jmse11040836

Gotoh, H., Shao, S., & Memita, T. (2004). SPH-LES model for numerical investigation of wave interaction with partially immersed breakwater. *Coastal Engineering Journal*, 46(1), 39–63. https://doi.org/10.1142/S0578563404000872

Han, Z., Liu, Z., & Shi, H. (2018). Numerical study on overtopping performance of a multi-level breakwater for wave energy conversion. *Ocean Engineering*, 150, 94–101. https://doi.org/10.1016/j.oceaneng.2017.12.058

Iuppa, C., Contestabile, P., Cavallaro, L., Foti, E., & Vicinanza, D. (2016). Hydraulic performance of an innovative breakwater for overtopping wave energy conversion. *Sustainability*, 8(12), 1226. https://doi.org/10.3390/su8121226

Monaghan, J. J. (2005). Smoothed particle hydrodynamics. *Reports on Progress in Physics*, 68(8), 1703–1759. https://doi.org/10.1088/0034-4885/68/8/R01

Monaghan, J. J. (1994). Simulating free surface flows with SPH. *Journal of Computational Physics*, 110(2), 399–406. https://doi.org/10.1006/jcph.1994.1034

Jiao, B., Zhao, Q., Chen, F., Liu, C., & Fang, Q. (2024). Numerical evaluation of wave dissipation on a breakwater slope covered by precast blocks with different geometrical characteristics. *Journal of Marine Science and Engineering*, 12(10), 1735. https://doi.org/10.3390/jmse12101735

Kerpen, N. B., Daemrich, K.-F., Lojek, O., & Schlurmann, T. (2020). Effect of variations in water level and wave steepness on the robustness of wave overtopping estimation. *Journal of Marine Science and Engineering*, 8(2), 63. https://doi.org/10.3390/jmse8020063

Kralli, V. E., Theodossiou, N., & Karambas, T. (2019). Optimal design of overtopping breakwater for energy conversion (OBREC) systems using the harmony search algorithm. *Frontiers in Energy Research*, 7, 80. https://doi.org/10.3389/fenrg.2019.00080

Lehmann, M., Karimpour, F., Goudey, C. A., Jacobson, P. T., & Alam, M. R. (2017). Ocean wave energy in the United States: Current status and future perspectives. *Renewable and Sustainable Energy Reviews*, 74, 1300–1313. https://doi.org/10.1016/j.rser.2016.11.101

Liu, Z., Shi, H., Cui, Y., & Kim, K. (2017). Experimental study on overtopping performance of a circular ramp wave energy converter. *Renewable Energy*, 104, 163–176. https://doi.org/10.1016/j.renene.2016.12.040

Mariani, A., Crispino, G., Contestabile, P., Cascetta, F., Gisonni, C., Vicinanza, D., & Unich, A. (2021). Optimization of low head axial-flow turbines for an overtopping breakwater for energy conversion: A case study. *Energies*, 14(15), 4618. https://doi.org/10.3390/en14154618

Martins, J. C., Goulart, M. M., Gomes, M. D. N., Souza, J. A., Rocha, L. A. O., Isoldi, L. A., & Dos Santos, E. D. (2018). Geometric evaluation of the main operational principle of an overtopping wave energy converter by means of constructal design. *Renewable Energy*, 118, 727–741. https://doi.org/10.1016/j.renene.2017.11.061

Musa, M. A., Ahmad, M. F., Roslan, M. F., Zulkifli, F., Fitriadhy, A., Nazri, M. N., Salleh, M. H., Rahman, M. A. A., & Mohd, M. H. (2021). Development of an experimental test for evaluating ramp shapes on overtopping breakwater for energy conversion. *Journal of Naval Architecture and Marine Engineering*, 18(1), 1–10. https://doi.org/10.3329/jname.v18i1.49209

Musa, M. A., Roslan, M. F., Ahmad, M. F., Muzathik, A. M., Mustapa, M. A., Fitriadhy, A., Mohd, M. H., & Rahman, M. A. A. (2020). The influence of ramp shape parameters on performance of overtopping breakwater for energy conversion. *Journal of Marine Science and Engineering*, 8(11), 875. https://doi.org/10.3390/jmse8110875

Nguyen, T. H., Hofland, B., Dan Chinh, V., & Stive, M. (2020). Wave overtopping discharge for very gently sloping foreshores. *Water*, 12(6), 1695. https://doi.org/10.3390/w12061695

Palma, G., Formentin, S. M., Zanuttigh, B., Contestabile, P., & Vicinanza, D. (2019). Numerical simulations of the hydraulic performance of a breakwater-integrated overtopping wave energy converter. *Journal of Marine Science and Engineering*, 7(2), 38. https://doi.org/10.3390/jmse7020038

Patrizi, N., Pulselli, R. M., Neri, E., Niccolucci, V., Vicinanza, D., Contestabile, P., & Bastianoni, S. (2019). Lifecycle environmental impact assessment of an overtopping wave energy converter embedded in breakwater systems. *Frontiers in Energy Research*, 7, 32. https://doi.org/10.3389/fenrg.2019.00032

Setayesh, P., & Moghim, M. N. (2025). An analytical-experimental study of wave overtopping in the OBREC device utilizing the maximum wave momentum flux

approach. *Ocean Engineering*, 337, 121879. https://doi.org/10.1016/j.oceaneng.2025.121879

Sujivakand, J., Jayakody, J. K. Y. A., Waharaka, W. V. A. M. N., Imantha, U. K. S., & Samarasekara, R. S. M. (2026). Enhancing coastal resilience and renewable energy generation: The role of breakwaters in wave energy extraction for sustainable development in Sri Lanka—a case study of Pandura breakwater. Journal of Ocean Engineering and Marine Energy, 12, 1035–1057. https://doi.org/10.1007/s40722-025-00457-y

Tedd, J., & Kofoed, J. P. (2009). Measurements of overtopping flow time series on the Wave Dragon wave energy converter. *Renewable Energy*, 34(3), 711–717. https://doi.org/10.1016/j.renene.2008.04.036

Trimulyono, A., Abror, I., Yudo, H., & Purwanto, D. B. (2023). Sensitivity analysis of SPH parameters for long-distance water wave propagation. In *IOP Conference Series: Earth and Environmental Science* (Vol. 1198, No. 1, 012001). https://doi.org/10.1088/1755-1315/1198/1/012001

Van Gent, M. R., Wolters, G., & Capel, A. (2022). Wave overtopping discharges at rubble mound breakwaters including effects of a crest wall and a berm. *Coastal Engineering*, 176, 104151. https://doi.org/10.1016/j.coastaleng.2022.104151

Vicinanza, D., Contestabile, P., Nørgaard, J. Q. H., & Andersen, T. L. (2014). Innovative rubble mound breakwaters for overtopping wave energy conversion. *Coastal Engineering*, 88, 154–170. https://doi.org/10.1016/j.coastaleng.2014.02.004

Wan, Z., Zheng, H., Sun, K., Zhang, D., Yao, Z., & Song, T. (2019). Simulation of wave energy converter with designed pendulor-slope combination. *Energy Procedia*, 158, 733–737. https://doi.org/10.1016/j.egypro.2019.01.196

Watanabe, M., Arikawa, T., Kihara, N., Tsurudome, C., Hosaka, K., Kimura, T., ... & Tateno, T. (2022). Validation of tsunami numerical simulation models for an idealized coastal industrial site. *Coastal Engineering Journal*, 64(2), 302–343. https://doi.org/10.1080/21664250.2022.2072611

Yasuda, T., Ueyama, H., & Mase, H. (2019). Empirical estimation of wave height over reef based on Boussinesq wave model. In *International Conference on Asian and Pacific Coasts* (pp. 175–181). Springer. https://doi.org/10.1007/978-981-15-0291-0_25

Zakaria, M. F. U. A. P., & Mukhtasor. (2025). State of the art of power take-off (PTO) systems in wave energy converter (WEC). *Ocean Engineering*, 335, 121669. https://doi.org/10.1016/j.oceaneng.2025.121669

Zhang, J., Zhang, N., Zhang, Q., Jiao, F., Xu, L., & Qi, J. (2022). Numerical simulation of wave overtopping of an ecologically honeycomb-type revetment with rigid vegetation. *Journal of Marine Science and Engineering*, 10(11), 1615. https://doi.org/10.3390/jmse10111615